OFFPRINT

Interface-driven magnetoelectric effects in granular CrO$_2$

A. Bajpai, P. Borisov, S. Gorantla, R. Klingeler, J. Thomas,
T. Gemming, W. Kleemann and B. Büchner

Please visit the new website
www.epljournal.org

TARGET YOUR RESEARCH WITH EPL

Sign up to receive the free EPL table of contents alert.

www.epljournal.org/alerts

Interface-driven magnetoelectric effects in granular CrO$_2$

A. Bajpai[1], P. Borisov[2], S. Gorantla[1], R. Klingeler[1,3], J. Thomas[1], T. Gemming[1], W. Kleemann[2] and B. Büchner[1]

[1] *Leibniz-Institute for Solid State and Materials Research, IFW Dresden - 01171 Dresden, Germany, EU*
[2] *Angewandte Physik, Universität Duisburg-Essen - 47048 Duisburg, Germany, EU*
[3] *Kirchhoff-Institute for Physics, Universität Heidelberg - 69120 Heidelberg, Germany, EU*

Abstract – Antiferromagnetic and magnetoelectric Cr$_2$O$_3$ surfaces strongly affect the electronic properties in half-metallic CrO$_2$. We show the presence of a Cr$_2$O$_3$ surface layer on CrO$_2$ grains by high-resolution transmission electron microscopy. The effect of these surface layers is demonstrated by measurements of the temperature variation of the magnetoelectric susceptibility. A major observation is a sign change at about 100 K followed by a monotonic rise as a function of temperature. These electric-field–induced moments in CrO$_2$ are correlated with the magnetoelectric susceptibility of pure Cr$_2$O$_3$. This study indicates that it is important to take into account the magnetoelectric character of thin surface layers of Cr$_2$O$_3$ in granular CrO$_2$ for better understanding the transport mechanism in this system. The observation of a finite magnetoelectric susceptibility near room temperature may find utility in device applications.

Introduction. – Advances in the field of spintronics are driven by the identification of materials with high degree of spin polarization (such as half-metalic ferromagnets) and materials in which magnetism can be tuned not only with an applied magnetic field but also through an applied electric field (magnetoelectric materials) [1–4]. This in turn has led to the study of composites of ferromagnetic and ferroelectric materials, which can exhibit properties superior to a single-phase compound [3].

A potential candidate for spintronic applications is CrO$_2$, which is a well-established half-metallic ferromagnet ($T_C \approx 393$ K) [5–8]. Owing to the large spin polarization value as well as it being a room temperature ferromagnet, CrO$_2$ is widely explored, both in thin films [7–12] and in bulk [13–15] form. A major limiting factor in realization of actual devices based on CrO$_2$ has been the issue of stability of its surface [9–15]. For instance, it easily converts to other stable oxides, such as Cr$_2$O$_3$. However, in case of granular CrO$_2$, it was recognised that this could be a rather advantageuos situation as far as magnetoresistive properties are concerned. The presence of Cr$_2$O$_3$ as an insulating surface layer makes granular CrO$_2$ a natural source of a magnetic tunnel junction [5,13,14]. This, together with the fact that Cr$_2$O$_3$ as the insulating surface

is both antiferromagnetic (AFM) and magnetoelectric (ME) [16–22] below $T_N \approx 307$ K in bulk, makes granular CrO$_2$ interesting from both the fundamental as well as the technological point of view. Correspondingly, this system provides the opportunity of a high spin polarization intrinsically associated with CrO$_2$ as well as of a significant magnetoelectricity arising from the Cr$_2$O$_3$ surfaces.

It is emphasized that while the phenomenon of magnetoelectricity is well established for Cr$_2$O$_3$ in the bulk single crystalline and polycrystalline forms [16,17,20], these features have not been explored when Cr$_2$O$_3$ appear as a grain boundary in granular CrO$_2$. In this work we first confirm the presence of the crystalline surface layer of Cr$_2$O$_3$ by TEM investigations. Further, we present direct experimental measurement of magnetoelectric susceptibility in granular CrO$_2$ in which Cr$_2$O$_3$ appears as a surface layer outside the CrO$_2$ grain.

Experimental details. – The sample is in the form of loosely sintered pellets of CrO$_2$, containing grains in the form of micron size rods. The synthesis and other characterization details can be found elsewhere [23]. It is important to note that these samples have shown much better magnetoresistive properties than commercial powders [24]. The transmission electron microscopic

(TEM) investigation on individual CrO_2 grains (derived from the same pellet) was performed using a FEI Tecnai F30 S-Twin. The measurements of the ME susceptibility have been performed using a superconducting quantum interference device (SQUID), MPMS-5S from Quantum Design, by modification of its ac susceptibility option [25]. The electrical conductivity has been measured in the standard four probe geometry, using a Quantum Design PPMS.

Results and discussions. –

Transmission electron microscopy measurements. For the TEM investigations, a single grain with a length of the order of a few μm and thickness of the order of 500 nm was isolated from the same pellet (fig. 1(a)) on which the ME susceptibility and resistivity measurements have been conducted. This sample shows a saturation magnetization of the order of 120 emu/g [23]. The TEM specimen is prepared by pressing a sparse layer of powder onto the grid and identifying isolated grains from the edges (fig. 1(b)). From the relatively thick grains a suitably thin edge was used for high-resolution transmission electron microscopy (HRTEM). Figure 1(b) shows an individual CrO_2 grain, the arrowhead in the figure represents the region from which the HRTEM image is obtained. The CrO_2 grain was tilted to the $[-111]$ zone axis using Kikuchi lines prior to HRTEM imaging which is shown in fig. 1(c). The fast Fourier transform (FFT) diffractogram from the highlighted region in fig. 1(c) was analyzed using the ELDISCA software [26], for determining the crystal structure. The surface layer is found to be polycrystalline Cr_2O_3, while no possible zone axis was found when a FFT diffractogram was analyzed with CrO_2 crystal structure. The presence of similar continuous Cr_2O_3 layers was observed along the edges of other CrO_2 grains.

The presence of Cr_2O_3 as a surface layer is consistent with the better tunneling magnetoresistance as observed in these samples [24]. Such a layer of low crystallinity has earlier been seen in TEM studies on commercial powders [14] and very recently in nanorods of CrO_2 [27], synthesized using our synthesis route [23]. However the direct observation of the crystalline Cr_2O_3 as a surface layer, such as shown in fig. 1(c), is rare.

Magnetoelectric susceptibility. The linear ME susceptibility α_{ij} is defined using $\mu_0 M_i \propto \alpha_{ij} E_j$ or $P_j \propto \alpha_{ij} H_i$, where M_i is the electric-field–induced magnetization and P_j is the magnetic-field–induced polarization [16]. In this work, we have measured the electric-field–induced magnetization. Our ME susceptibility measurements are conducted by applying an ac voltage, $u(t) = u_0 \cos \omega t$ across the sample and measuring the induced ac magnetic moment, $m(t) = m' \cos \omega t + m'' \sin \omega t$ in zero external magnetic field. The schematic of the measurement, which can be done in both *constant applied voltage amplitude* ($u_0 = $ const) and *constant applied current amplitude* mode ($i_0 = $ const), is shown in fig. 2. The details of the measurement procedure can be found elsewhere [25]. The
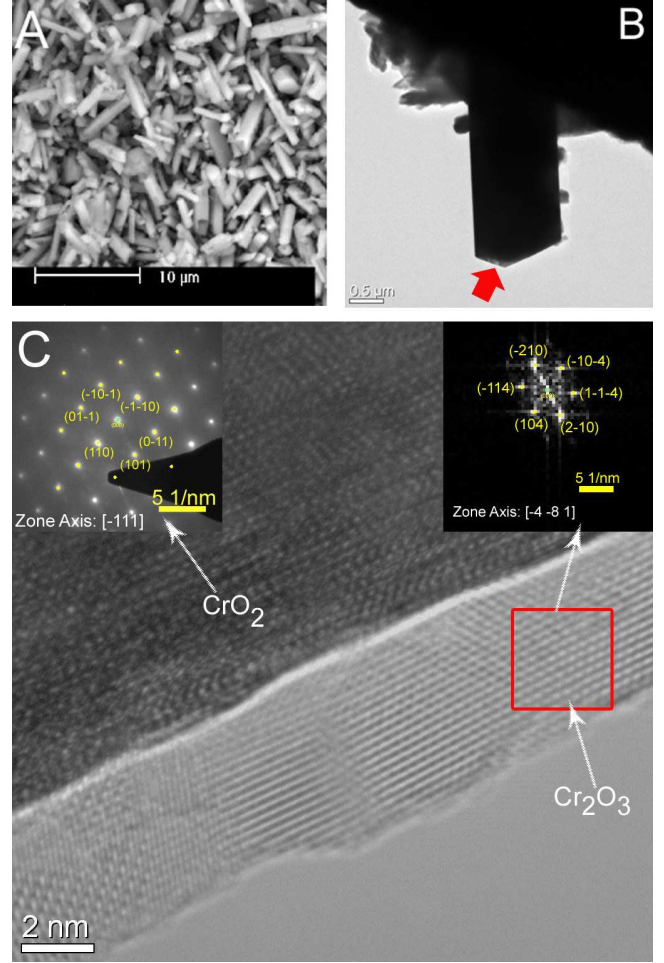

Fig. 1: (Colour on-line) (a) SEM image of a pellet containing the CrO_2 grains in the shape of micron size rods. The bright field TEM image of an individual CrO_2 grain is shown in (b). The HRTEM image of CrO_2 grain with Cr_2O_3 oxide layer is shown in (c). The right inset in (c) shows the FFT diffractogram, extracted from the region represented by the rectangular box in (c), overlaid by the calculated diffraction pattern for the $[-4 - 8 \ 1]$ zone axis of Cr_2O_3. The left inset shows the experimental diffraction pattern of CrO_2 grain overlaid by a calculated pattern for the $[-111]$ zone axis.

lower panel of fig. 2 shows a complex plane representation of the real (m') and the imaginary (m'') part of the ME susceptibility as measured on the CrO_2 sample at $i_0 = $ const mode at 10 Hz.

Figure 3(a) shows the real part of the electric-field–induced moment as a function of temperature for granular CrO_2. The data are obtained in both cooling and heating cycles, measured in constant-current-amplitude mode. The moments exhibit a change of sign below 100 K, followed by a rapid rise in magnitude up to the maximum temperature of 350 K. A substantial thermal hysteresis is observed in cooling and heating cycles, which becomes pronounced above 200 K. Figure 3(b) compares the ME susceptibility in a single crystal of Cr_2O_3 (blue stars)
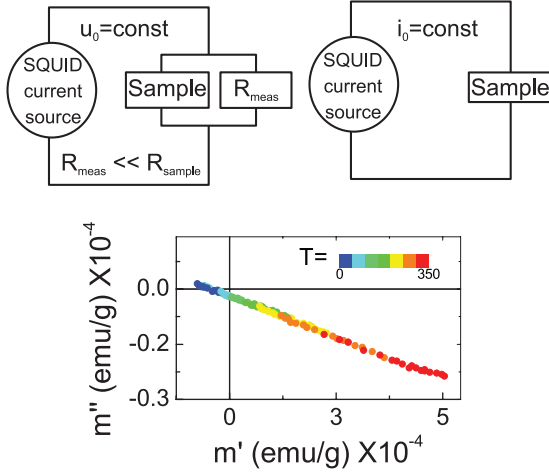
Fig. 2: (Colour on-line) The upper left panel depicts the schematic of the ME susceptibility measurement in constant-voltage-amplitude mode, while the upper right panel shows the same in constant-current-amplitude mode. The lower panel displays the complex plane representation (m'' vs. m') of the real and the imaginary parts of the electric-field–induced moment as measured in granular CrO$_2$ at different temperatures.

Fig. 3: (Colour on-line) (a) Temperature dependence of the real part of the electric-field–induced moment (m') in cooling and heating cycles, showing thermal hysteresis and a change of sign around 100 K. (b) m' in a single crystal of Cr$_2$O$_3$ (blue stars) and granular CrO$_2$ (red circles). The data set on Cr$_2$O$_3$ is multiplied by a factor of 10. (c) Resultant amplitude of the moment varying linearly as a function of the applied-electric-field amplitude at 263 K.

with that measured on the granular CrO$_2$ (red circles). Both measurements were performed in heating cycle using the same experimental set up. The ac electric-field amplitude for granular CrO$_2$ and Cr$_2$O$_3$ were 1 V/m and 63 kV/m, respectively. In addition, the single crystal of Cr$_2$O$_3$ was ME annealed in the magnetic field of 6000 Oe and in dc electric field of 300 kV/m [25] whereas no annealing fields were required for CrO$_2$. The data on Cr$_2$O$_3$ are multiplied by a factor of 10 so as to compare its temperature variation with that measured on granular CrO$_2$. This comparison reveals that in both cases the ME signal changes sign at about 100 K. However, unlike what is observed in pure Cr$_2$O$_3$, the ME moments in granular CrO$_2$ do not vanish at the T_N of Cr$_2$O$_3$, but continue to rise further till the measured temperature of 350 K. Figure 3(c) shows that the resultant moment exhibits a linear variation as a function of the applied-electric-field amplitude measured at a fixed temperature, as is expected for linear ME effects, typically seen in pure Cr$_2$O$_3$.

We first focus our attention to the change of sign in ME moments at about 100 K. It is to be noted that the sign of the induced moments for such measurements is arbitrary, but is fixed for a particular connection during a run. Therefore, the change of sign during one set of run is not arbitrary. It is recalled that the ME susceptibility measured on pure Cr$_2$O$_3$ shows a similar change of sign at around 100 K, which is well documented in the literature [16,19,25]. This feature in pure Cr$_2$O$_3$ is understood to arise from an interplay between a two-ion term (electrically induced change in the exchange interactions in sublattices that disturbs the mutual compensation of antiparallel spins) and a single-ion term (due to the
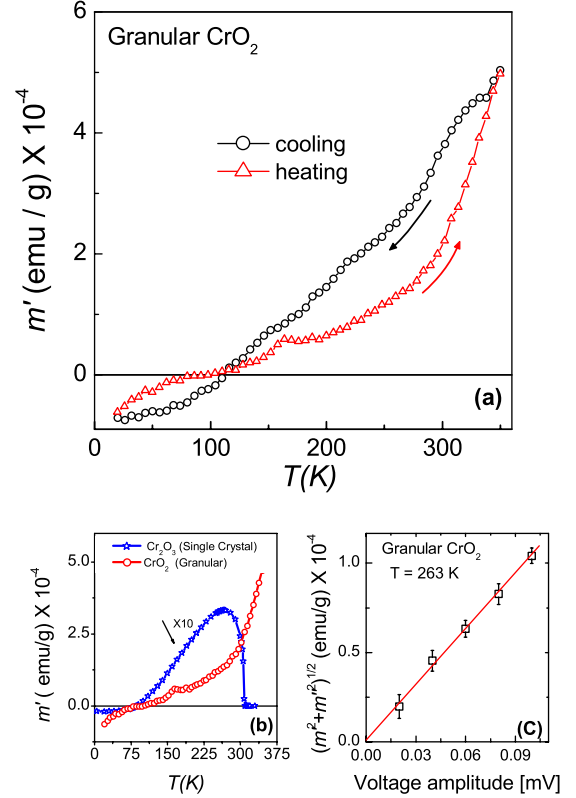
electric-field–induced g-shift) which have opposite signs. Although Cr$_2$O$_3$ appears only as grain boundary in granular CrO$_2$, both of them, granular CrO$_2$ and pure Cr$_2$O$_3$ exhibit a change of sign in the ME susceptibility, occurring in a similar temperature range and this feature is indicative of strong interface effects. This provides compelling evidence that the ME response in granular CrO$_2$ is modulated by features intrinsic to the pure Cr$_2$O$_3$ phase.

We also observe that the ME signal is much larger in magnitude in relatively small applied electric field in CrO$_2$ and no magnetoelectric annealing is required as in case of Cr$_2$O$_3$. A rough attempt to extract the size of the corresponding magnetoelectric coupling for CrO$_2$ yields α ($\approx \mu_0 M_z / E_z$) in the order of 10^{-7} s/m. This estimation is based on the experimentally observed electric-field–induced moment (m') and secondary effects such as the anisotropy of the ME effect, AFM domains and the polycrystalline nature of our sample have been neglected. This value is about 5 orders of magnitude larger than the maximal value of α for the pure Cr$_2$O$_3$ which exhibits $\alpha_{zz} \approx 4$ ps/m [16,17,25]. However, we emphasize
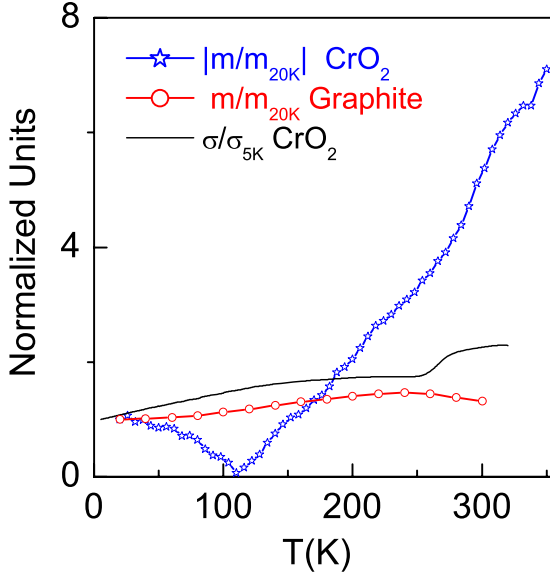
Fig. 4: (Colour on-line) Comparison of normalized values of electric-field–induced moment recorded in cooling cycle for CrO$_2$ sample (blue stars) and a graphite sheet (red circles) having resistivity in similar range with that of CrO$_2$ sample. The black line is the normalized conductance of CrO$_2$ measured in the bias current of 100 μA.

that any comparison of α, *e.g.*, for the two samples studied at hand, should be taken very cautiously.

In this context, it is important to recall that while Cr$_2$O$_3$ is insulating, granular CrO$_2$ shows activated transport with relatively low resistivity values of the order of a few Ωcm [24,28]. This may lead to additional contributions to the ME effect and need to be distinguished from the classical ME effects intrinsic to pure Cr$_2$O$_3$. For instance, the low resistivity of our samples may lead to generation of moments induced due to the surface currents, which we refer to as the Oersted moment, to differentiate it from ME response. During a ME measurement at a constant current amplitude, this contribution should be independent of the temperature —if we ignore the modulations driven by the ferromagnetic interactions.

In order to investigate the possible effect of Oersted moments, we conducted an experiment in the same configuration on a graphite sample. This sample consists of thin graphite sheets, commercially available from Goodfellow and three such sheets were glued together by silver paste so that the resistivity of this sample is of the order of a few Ωcm, similar to the CrO$_2$ sample. The sample geometry was similar to the CrO$_2$ sample, too. In fig. 4, we compare the normalized electric-field–induced moments as observed in a cooling cycle for both the granular CrO$_2$ ($i_0 = 125\,\mu$A = const) and the graphite sample ($i_0 = 175\,\mu$A = const). The data indeed imply the presence of finite Oersted moments in the graphite model sample. However, the observed moments in the graphite sample show no change of sign and they are temperature

independent. This is unlike what is observed in granular CrO$_2$. Thus, although Oersted moments may affect the magnitude of the observed signal, these contributions cannot explain the strong temperature dependence of the electric-field–induced moments as is seen in granular CrO$_2$.

We also note that it is nontrivial to estimate the magnitude of surface currents in our sample with randomly oriented grains with insulating grain boundary. Though we have tried to estimate the maximal possible magnitude of ME moments, taking into account the Cr$_2$O$_3$ surface layer outside the grains[1]. These calculations show that the magnitude of the ME moments is still 4 to 5 orders of magnitude smaller than what is observed experimentally and therefore the exact scenario cannot be understood unless interface effects are taken into accout.

We also plot the normalized conductance measured at a fixed bias current of 100 μA for granular CrO$_2$ in the same graph (fig. 4). This comparison reveals that the functional form of the observed moments in granular CrO$_2$ is strikingly different from what is expected from the surface currents associated to the Oersted moment. The observation of change of sign was also reconfirmed by measurements repeated in both constant-current-amplitude (fig. 4, $i_0 = 125\,\mu$A) and constant-voltage-amplitude mode (not shown). These experimental observations strongly indicate that the origin of electric-field–incuced moments in our sample is correlated with ME effects in Cr$_2$O$_3$.

While change of sign as well as linear variation of moments as a function of electric field (fig. 3(c)) point towards the modulation driven by AFM/ME Cr$_2$O$_3$, the continuous increase of the moment as a function of temperature right up to 350 K is puzzling. This is contrary to what is seen in the pure Cr$_2$O$_3$ phase where the ME moment vanishes at T_N of Cr$_2$O$_3$ (307 K). Though such effects are not uncommon and plenty of work —particularly in tailor-made FM/AFM systems— reports unusual exchange bias effects that exist beyond the Néel temperature of its AFM component [29–31]. These features are usually attributed to strain or proximity effect and we also have seen some manifestations in our samples [32]. However, the exact physical mechanisms that leads to such observation are not well explored.

In this context, it is recalled that in general, the microscopic origin of ME effects is understood to arise from four basic mechanisms such as g-tensor, single-ion anisotropy, symmetric and antisymmetric exchange mechanism [33,34]. Depending on the strength of interaction, the total ME effect is governed by one of these mechanisms or their combinations. For instance, the two-ion

---

[1]Under assumptions that the CrO$_2$ sample consists of spherical grains with average diameter of 5 μm and with grain boundaries layer of 2 nm Cr$_2$O$_3$, the electric-field drop at the grain interface is about 10^3 times the external electric field. As the volume ratio of Cr$_2$O$_3$ outside a single grain is about 10^{-3}, the total electrically induced moment is finally the same as in the case of 100% Cr$_2$O$_3$.

contribution, related to a net change in the bulk magnetization of AFM, arising due to the inequivalence of the two sublattices on application of the electric field, vanishes above the Néel temperature. However, the ME annealing effects as observed in pure Cr$_2$O$_3$ are explained in terms of the atomic single-ion ME coefficients which exist in the paramagnetic regime (*i.e.* above 307 K) in Cr$_2$O$_3$ but this effect is enhanced when long-range AFM order sets in [21]. The usual ME effect (related to the AFM order) is itself a weak effect and to observe the change due to individual moments is even more challenging. However, it is in principle possible to observe the ME effect related to the change in the magnitude of an individual moment on application of the electric field [33,34].

In our case, the Cr$_2$O$_3$ appears at the interface of another long-range ordered magnet (CrO$_2$), whose T_C is about 400 K. In this situation, the ME moments arising due to single-ion ME coefficients of Cr$_2$O$_3$ may still be finite above T_N, due to proximity effects [27,35]. Though we could measure the ME moments up to about 350 K, we speculate that they may eventually diminish only above 400 K. Prior experimental data on thin films of CrO$_2$ having a surface layer of Cr$_2$O$_3$ as well as bilayers of CrO$_2$/Cr$_2$O$_3$ have also shown some interesting interface effects [35,36].

This study indicates that it is important to explore the influence of the AFM/ME character of Cr$_2$O$_3$ when it appears at the interface, particularly in transport measurements. In these samples, we do see unusual thermal history and bias current effects in resistivity measurements (unpublished). These data also point towards the need to take into account the ME character of the grain boundary in order to understnd the transport mechanism in this system.

In conclusion, from direct measurement of high-resolution transmission electron microscopy we show that our CrO$_2$ grains contain a surface layer of *polycrystalline* Cr$_2$O$_3$. This can account for the much improved tunneling magnetoresistance as has earlier been observed in these samples. The influence of the magnetoelectric character of the surface layer is visible in magnetoelectric susceptibility measurements. The observation of finite electric-field–induced moments right up to 350 K in granular CrO$_2$ can be understood to arise from interface effects, taking into account the modulations driven by the ME character of Cr$_2$O$_3$. A finite ME susceptibility at room temperature may prove to be useful in CrO$_2$ based devices.

* * *

REFERENCES

[1] CHEONG S.-W. and MOSTOVOY M., *Nat. Mater.*, **6** (2007) 13.
[2] RAMESH R. and SPALDIN N. A., *Nat. Mater.*, **6** (2007) 21.
[3] FIEBIG M., *J. Phys. D: Appl. Phys.*, **38** (2005) R123.
[4] DÖRR K., *J. Phys. D: Appl. Phys.*, **39** (2006) R125.
[5] HWANG H. Y. and CHEONG S.-W., *Science*, **278** (1997) 1607.
[6] GROOT R. A. *et al.*, *Phys. Rev. Lett.*, **50** (1983) 2024.
[7] SOULEN R. J. *et al.*, *Science*, **282** (1998) 85.
[8] PARKER J. S., WATTS S. M., IVANOV P. G. and XIONG P., *Phys. Rev. Lett.*, **88** (2001) 196601.
[9] SPINU L., SRIKANTH H., GUPTA A., LI X. W. and GANG XIAO, *Phys. Rev. B*, **62** (2000) 8931.
[10] IVANOV P. G., WATTS S. M. and LIND D. M., *J. Appl. Phys.*, **89** (2001) 1035.
[11] RUEDIGER U. *et al.*, *J. Appl. Phys.*, **89** (2001) 7699.
[12] IVANOV P. G. and BUSSMANN K. M., *J. Appl. Phys.*, **105** (2007) 07B107.
[13] COEY J. M. D. *et al.*, *Phys. Rev. Lett.*, **80** (1998) 3815.
[14] DAI J. *et al.*, *Appl. Phys. Lett.*, **77** (2000) 2840.
[15] DAI J. and TANG J., *Appl. Phys. Lett.*, **63** (2001) 064410.
[16] RADO G. T. and FOLEN V. J., *Phys. Rev. Lett.*, **7** (1961) 310.
[17] ASTROV D. N., *Sov. Phys. JETP*, **11** (1960) 708.
[18] FOLEN V. J., RADO G. T. and STALDER E. W., *Phys. Rev. Lett.*, **6** (1961) 607.
[19] HORNREICH R. and SHTRIKMAN S., *Phys. Rev.*, **161** (1961) 506.
[20] SHTRIKMAN S. and TREVES D., *Phys. Rev.*, **130** (1963) 986.
[21] MARTIN T. J. and ANDERSON J. C., *Phys. Lett.*, **11** (1964) 109.
[22] BROWN P. J. *et al.*, *J. Phys.: Condens. Matter*, **10** (1998) 663.
[23] BAJPAI A. and NIGAM A. K., US Patent 7276226.
[24] BAJPAI A. and NIGAM A. K., *Phys. Rev. B*, **75** (2007) 064403.
[25] BORISOV P. *et al.*, *Rev. Sci. Instrum.*, **78** (2007) 106105.
[26] THOMAS J. and GEMMING T., in *Proceedings of the EMC 2008: 14th European Microscopy Congress, 1–5 September 2008, Aachen, Germany*, edited by MAYER J. *et al.* (Springer) 2008, ISBN 978-3-540-85301-5, p. 231.
[27] SONG Y., SCHMITT A. L. and SONG JIN, *Nano Lett.*, **8** (2008) 2356.
[28] BAJPAI A. and NIGAM A. K., *J. Appl. Phys.*, **101** (2007) 10391.
[29] SAHOO S. *et al.*, *Appl. Phys. Lett.*, **91** (2007) 172506.
[30] SHI H. *et al.*, *Phys. Rev. B*, **69** (2004) 214416.
[31] VAN DER ZAAG P. J. *et al.*, *Phys. Rev. Lett.*, **84** (2000) 6102.
[32] BAJPAI A. *et al.*, *J. Phys.: Condens Matter*, **22** (2010) 096005.
[33] DE ALCANTARA BONFIM O. F. and GEHRING G. A., *Adv. Phys.*, **29** (1980) 731.
[34] GEHRING G. A., *Ferroelectrics*, **161** (1993) 275.
[35] CHENG R. *et al.*, *Phys. Lett.*, **A302** (2008) 21.
[36] FREY N. A. *et al.*, *Phys. Rev. B*, **74** (2006) 024420.